


Electrodeposited Cu-Sn Alloy for Electrochemical CO₂ Reduction to CO/HCOO⁻

Masayuki Morimoto^{1,2} · Yoshiyuki Takatsuji^{1,2} · Ryota Yamasaki^{1,2,3} · Hikaru Hashimoto^{1,2} · Ikumi Nakata^{1,2} · Tatsuya Sakakura¹ · Tetsuya Haruyama^{1,2,3} 

Published online: 1 November 2017

© The Author(s) 2017. This article is an open access publication

Abstract Cu-Sn alloy electrodes were prepared by simple electrodeposition method for the electrochemical reduction of CO₂ into CO and HCOO⁻. The alloy electrode surfaces provided good selectivity and efficiency in electrochemical CO₂ conversion because they provided appropriate binding energies between the metal and the reactive species obtained through CO₂ reduction. Therefore, product selectivity can be modulated by altering the Cu-Sn crystal structure of the electrode. Using the Cu-Sn alloy electrodes, electrochemical reduction was performed at applied potentials ranging from -0.69 to -1.09 V vs. reversible hydrogen electrode (RHE). During electrochemical CO₂ reduction, all the prepared Cu-Sn alloy electrodes showed prominent suppression of hydrogen evolution. In contrast, Cu₈₇Sn₁₃ has high selectivity for CO formation at all the applied potentials, with maximum faradaic efficiency (FE) of 60% for CO at -0.99 V vs. RHE. On the other hand, Cu₅₅Sn₄₅ obtained a similar selectivity for electrodeposition of Sn, with FE of 90% at -1.09 V vs. RHE. Surface characterization results showed that the crystal structure of Cu₈₇Sn₁₃ comprised solid solutions that play an important role in increasing the selectivity for CO formation. Additionally, it suggests that the selectivity for HCOO⁻

formation is affected by the surface oxidation state of Sn rather than by crystal structures like intermetallic compounds.

Keywords CO₂ reduction · CO₂ conversion · Cu-Sn alloy · Product selectivity · Carbon monoxide · Formic acid

Introduction

Greenhouse gases have recently garnered great attention from the viewpoint of global warming and climate change. Since CO₂ gas is a greenhouse gas, CO₂ reduction is required to address the global issue of increasing CO₂ emission [1]. To this end, many researchers have undertaken CO₂ reduction and conversion to energetic compounds by chemical, biological, photochemical, inorganic, and electrochemical approaches [2–4]. Among these approaches, the electrochemical reduction of water-dissolved CO₂ in the presence of a metal catalyst can generate CO, HCOO⁻, and hydrocarbons with high current efficiency and high reaction selectivity [5–7]. The products obtained from CO₂ depend on the metal species used as the catalyst. Cu as CO₂ reduction reaction (CO₂RR) catalyst generates hydrocarbons including C₁, C₂, and C₃ products [7–9]. Au, Ag, Pd, and Zn catalysts provide high selectivity for CO production and HCOO⁻ is the major product obtained with Sn, Hg, and Pb catalysts [5, 6, 10]. In the presence of other metal catalysts, hydrogen evolution reaction (HER) occurs preferentially compared to CO₂RR [5]. This product selectivity is due to the binding energy of CO₂ and its reaction intermediates to the metal species, as confirmed by density functional theory (DFT) studies [7, 10–12]. Binding energy was also affected by the crystal face and valence of

✉ Tetsuya Haruyama
haruyama@life.kyutech.ac.jp

¹ Division of Functional Interface Engineering Department of Biological Functions Engineering, Kyushu Institute of Technology, Kitakyushu Science and Research Park, Fukuoka 808-1096, Japan
² Advanced Catalytic Transformation Program for Carbon Utilization (ACT-C), Japan Science and Technology Agency (JST), Tokyo 102-0076, Japan
³ Research Center for Advanced Eco-Fitting Technology, Kitakyushu Science and Research Park, Fukuoka 808-1096, Japan

metals such as Cu and Cu₂O [13–16]. In other words, for highly efficient and selective CO₂RR, we need to design catalysts considering the binding energy of CO₂ and its reaction intermediates to the catalyst surface.

CO₂RR activity of Cu electrode has attracted attention over the year because it can produce hydrocarbons like methane, ethylene, methanol, and ethanol with a relatively high efficiency. In polycrystalline Cu, CO formation competes with HCOO[−] formation at applied potentials less than −0.9 V vs. reversible hydrogen electrode (RHE). Hydrocarbons formation starts at −0.9 V and ethylene is formed first, followed by methane. At applied potentials more negative than −0.9 V, methane formation dominates over ethylene formation, and the formation of ethanol, methanol, and C₃ products starts. The HER competes directly with CO₂RR but decreases with increasing applied potential [8, 9]. On the other hand, in Cu single-crystal electrode, product selectivity of CO₂RR depends on the Cu crystal surface [13], suggesting that changes in deficiency of surface, step, and edge have a significant effect on product selectivity [9]. In addition, Cu₂O possesses high selectivity for ethylene formation due to the significant inhibition of methane formation [15, 16]. At present, the factor responsible for changing C₁ and C₂ selectivity is not evident; however, the aforementioned results yield useful knowledge in terms of selectivity control.

DFT calculations have established that the selectivity of CO₂RR is enhanced by using alloys [17–19]. Alloying controls the binding energy of the CO₂RR reactive species to the electrode surface by changing the metal species and content ratio. Kortlever et al. reported that altering the composition of Pd and Pt in the Pd_xPt_(100-x)/C catalyst led to a major change in HCOO[−] selectivity [20]. Among Cu-based alloy catalysts, oxide-derived Cu_xZn prepared by electroplating possesses high selectivity for ethanol formation with faradaic efficiency (FE) of ~30%, as reported by Ren et al. [21]. Meanwhile, CuInO₂ prepared by electrophoretic deposition showed increased CO selectivity compared to Cu₂O [22]. Moreover, Cu-Sn catalyst achieved CO production FE of ~90% by changing the deposition amount of Sn on oxide-derived Cu surface. This results in suppressed H₂ and HCOO[−] formation, as confirmed by DFT calculations [23]. However, the cause for increasing selectivity due to the formation of Cu-Sn alloy is not clear. The dependence of selectivity on alloy composition was also not clarified.

When CO₂RR was performed on commercial Sn electrode, FE of HCOO[−] production was over 91% in 0.1 M KHCO₃ at −1.8 V vs. Ag/AgCl [24]. Moreover, for Sn electrodeposited on Cu plate, FE of HCOO[−] varied with Sn electrodeposition thickness and it was 91% at −1.4 V vs. SCE [25]. As mentioned earlier, Sn has high selectivity toward HCOO[−]. This phenomenon suggested that the surface oxide of Sn plays an important role in HCOO[−] formation. It has been reported that Sn etched with HBr showed significantly low FE for HCOO[−]

production compared with untreated Sn electrode in 0.5 M NaHCO₃ at −0.7 V vs. RHE [26]. The relation between the valence of Sn and CO₂RR activity is unclear because Sn is susceptible to oxidation.

In this study, we focused on an electrode coated with electrodeposited Cu-Sn alloy for CO₂ electroreduction catalysts. There are many reports on co-deposition of two metal catalysts to improve selectivity, but we control reaction products from the standpoint of alloy structures like solid solutions or intermetallic compounds. Specifically, we proposed to control product selectivity of CO and HCOO[−] by changing the crystal structure and alloy composition ratio of Cu and Sn, respectively. The Cu-Sn alloy electrode was prepared using an electroplating method and the composition ratio was adjusted by altering the molar ratio of the Cu-Sn electrolyte. Surface characteristics of the Cu-Sn catalysts were analyzed using scanning electron microscopy (SEM), X-ray diffraction (XRD), X-ray photoelectron spectroscopy (XPS), and Auger electron spectroscopy (AES). Our study shows that the Cu-Sn alloy can control product selectivities of CO and HCOO[−] by altering the alloy composition. The effect of alloy composition on the selectivity for CO₂RR was also discussed.

Experimental

Electrodeposition of Cu-Sn Alloy

The Cu-Sn alloy catalysts were prepared by the electrodeposition method. All the prepared catalyst electrodes used Cu plate (T=0.2 mm, Nillaco Corp.) as the substrate. The Cu plate was washed three times by ultrasound in acetone and then was similarly rinsed with ultrapure water. It was then immersed in 1 M HCl for 30 s and dried by N₂ followed by rinsing with ultrapure water before use as the working electrode (WE). The electrolyte consisted of 0.5 M K₄P₂O₇ (97%, Sigma-Aldrich Co. LLC), 0.05 M C₆H₁₄N₂O₇ (99.0%, Sigma-Aldrich Co. LLC), and varying concentrations of CuSO₄·5H₂O (99.5%, Wako Ltd.) and SnSO₄ (96%, Wako Ltd.), such that the total concentration of metals was 0.2 M dissolved in ultrapure water. The electrodeposition on the Cu substrate was carried out using a two-electrode system where the counter electrode (CE) was a Pt plate. To study the effect of Cu-Sn alloy catalysts on CO₂ reduction activity, we employed Cu and Sn electrodeposited electrodes. The electrolyte for Cu electrodeposition comprised 0.5 M K₄P₂O₇, 0.2 M C₄H₁₂N₂O₅ (99.0%, Sigma-Aldrich Co. LLC), and 0.2 M CuSO₄·5H₂O dissolved in ultrapure water. The Sn electrodeposition electrolyte comprised 0.5 M K₄P₂O₇, 0.2 M SnSO₄, 1 g/L PEG 6000 (Wako Ltd.), and 0.6 mL/L formalin. The prepared catalysts were washed with ultrapure water and dried N₂. The electrodeposition conditions for various Cu-Sn alloys, Cu, and Sn on Cu substrate are shown in Table 1.

Table 1 Electrodeposition condition of various catalysts. The composition ratio of each Cu-Sn alloy was decided by AES analysis

	Cu	Cu ₈₇ Sn ₁₃	Cu ₇₆ Sn ₂₄	Cu ₅₅ Sn ₄₅	Sn
K ₄ P ₂ O ₇ (M)	0.5	0.5	0.5	0.5	0.5
C ₆ H ₁₄ N ₂ O ₇ (M)		0.05	0.05	0.05	
C ₄ H ₁₂ N ₂ O ₅ (M)	0.2				
CuSO ₄ ·5H ₂ O (M)	0.2	0.18	0.16	0.1	
SnSO ₄ (M)		0.02	0.04	0.1	0.2
PEG 6000 (g/L)					1
Formalin (mL/L)					0.6
Current density (mA/cm ²)	5.6	3.2	3.2	3.6	1
Deposition time (min)	5	5	5	5	5

Characterization of Prepared Catalysts

To determine the composition ratio of the prepared Cu-Sn catalysts before and after CO₂ electroreduction, they were analyzed by AES (JEOL Ltd., JAMP-7810). The X-ray source used an LaB₆ filament. The surface morphology of the prepared catalysts was analyzed before and after CO₂ reduction using SEM (JEOL Ltd., JSM-6701). The crystal face and structure of the Cu-Sn alloy was evaluated before and after CO₂ reduction by thin-film XRD (MAC Science, MO3XHF22) technique. The X-ray source used Cu K α ($\lambda = 0.154$ nm, 30 mA) and the scan angle recorded at 2θ value between 25° and 80° in steps of 0.2°. The chemical bonding states of Cu 2p and Sn 3d were analyzed before and after CO₂ reduction by XPS (Shimadzu Co., KRATOS AXIS-NOVA) with Al K α as the X-ray source. The obtained binding energies of Cu 2p and Sn 3d orbitals were calibrated with the C–C bond of carbon contamination as a reference at 284.2 eV.

Electrochemical Reduction of CO₂

A custom-made two-compartment electrolysis cell made from acrylic plastic was used (Fig. 1). The Pt plate and Ag/AgCl (3.3 M KCl) were used as the CE and reference electrode (RE), respectively. The cathode was separated from the anode by a cation-exchange membrane (Nafion NRE-212, Sigma-Aldrich Co. LLC). The electrolyte (23 mL) used was 0.1 M KHCO₃ (99.5%, Wako Ltd.) solution saturated with CO₂ gas (99.995%, JFP) for 40 min. The CO₂ gas flowed continuously during the CO₂ electroreduction at a flow rate of 5 mL/min. The electrolyte was stirred by a stirring bar.

In the electrochemical measurements, the potential and current were controlled or measured using a potentiostat (Hokuto Denko Corp., HZ-7000) and the IR drop was corrected. In this study, the Ag/AgCl was converted to a reversible hydrogen electrode (RHE) at all potentials using the following formula: $E_{\text{RHE}} = E_{\text{Ag/AgCl}} + 0.210 + (0.0591 \times \text{pH})$. Here, the pH of CO₂-saturated 0.1 M KHCO₃ solution was 6.8. The

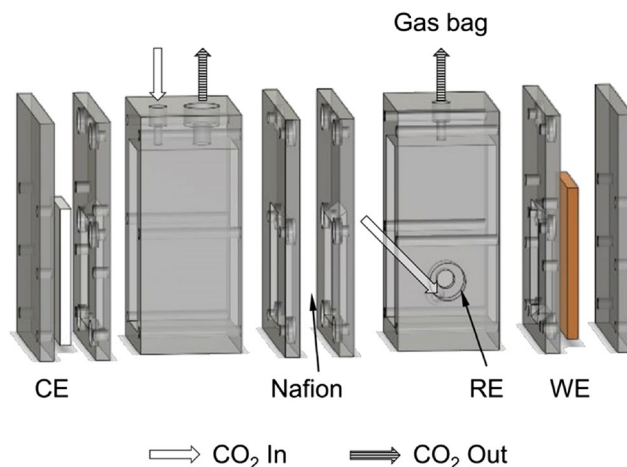


Fig. 1 Schematic of the electrolysis cell used for CO₂ reduction. WE, working electrode; RE, reference electrode; CE, counter electrode

electrochemical CO₂ reduction was performed using controlled potential chronoamperometry for 1800 s and the applied potential was in the range from -0.69 to -1.09 V vs. RHE. The FE of the products from CO₂ reduction was calculated based on Eq. (1).

$$\text{FE} = \frac{z n F}{Q} \times 100 \quad (1)$$

Where, z is the number of electron transfers needed for CO₂ reduction, n is the number of moles from the results of the quantitative analyses, F is the Faraday constant (96,485 C/mol), and Q is the amount of electricity.

The gaseous products formed by CO₂ electroreduction and the introduced CO₂ gas were collected by a connected gas bag (Smart Bag PA, GL Sciences Inc.) and the head space of the electrolysis cell. The collected gas was analyzed by gas chromatography (GC, Shimadzu Co., Tracera). We used Micropacked ST (Shinwa Chemical Industries Ltd.) as the GC column and He (Iwatani Corp.) used as the carrier gas. The HCOO⁻ content in the liquid products obtained after CO₂ reduction was analyzed by anion chromatography (IC, Shimadzu Co., Prominence HIC-SP) after dilution with ultra-pure water. The column employed for IC was Shim-pack IC-SA3 (Shimadzu Co.) and the eluting solution was 3.6 mM Na₂CO₃ (99.5%, Wako Ltd.) solution. The prepared electrodes were used for electrochemical CO₂ reduction just once. In this study, the FE of gaseous and liquid products was the mean amount of time spent on the CO₂ reduction. Additionally, FE of the products was obtained by averaging the results of the experiments three times with CO₂ reduction on each electrode.

Electrochemical Impedance Spectroscopy

The electrochemical impedance spectroscopy (EIS) was carried out under the same conditions as those used for CO₂

electroreduction condition at -0.89 and -1.09 V vs. RHE in 0.1 M KHCO_3 solution employed by the potentiostat. Before applying the AC amplitude potential, the cathode was kept at -0.89 or -1.09 V for 120 s to become stabilized to the current through the sample. The AC amplitude potential and measurement potential were set at 100 mV and -0.89 or -1.09 V, respectively, and the measurement frequency was scanned in a range of 100 kHz to 500 mHz.

Results and Discussion

Characterization of Cu-Sn Alloy Catalysts

The composition ratio of Cu and Sn in the prepared Cu-Sn catalysts was determined before and after CO_2 reduction using AES measurement (Table 2). In this paper, the prepared Cu-Sn catalysts are described as $\text{Cu}_{87}\text{Sn}_{13}$, $\text{Cu}_{76}\text{Sn}_{24}$, and $\text{Cu}_{55}\text{Sn}_{45}$, based on AES results. The Cu and Sn deposited electrodes are described as Cu_{100} and Sn_{100} , respectively. AES Cu signal on the Sn_{100} electrode originated from the Cu substrate or diffusion of the Cu to deposited Sn [27, 28]. Any detected element apart from Cu and Sn was considered contamination from ambient air or oxide on the metal surface. Table 2 shows that the relative composition ratio of oxygen increased with increasing ratio of Sn due to Sn being more susceptible to oxidation than Cu. After CO_2 reduction at -0.89 V vs. RHE for 30 min, the Cu-Sn ratio of the Cu-Sn catalysts slightly increased due to diffusion of Cu and Sn upon applying the reduction potential, as suggested by the SEM and XRD results after CO_2 reduction [27, 28].

Figure 2a–j shows the SEM images of electrodeposited Cu and Sn on the Cu substrate. Cu_{100} and Sn_{100} comprise distributed particles with size of ~ 300 nm. The Cu-Sn catalysts, except $\text{Cu}_{55}\text{Sn}_{45}$, have uniformly dense structures and particle size decreased with increasing Cu concentration. $\text{Cu}_{55}\text{Sn}_{45}$

showed a unique surface morphology and crystal growth was complicated. After CO_2 reduction at -0.89 V vs. RHE for 30 min, the macroscale morphologies of all the catalysts remained unchanged. The Cu_{100} revealed particle abrasion, but particle size did not change before and after CO_2 reduction. On the other hand, Sn_{100} exhibited cohesion and spalling of particles throughout the surface. Correspondingly, $\text{Cu}_{55}\text{Sn}_{45}$ and $\text{Cu}_{87}\text{Sn}_{13}$ were examined for deposition of small particles on the catalyst surface.

The crystalline structures of the Cu-Sn catalysts deposited on Cu plate were analyzed by XRD before and after CO_2 reduction (Fig. 3). All the catalysts exhibiting Cu diffraction peak originated from the substrate. Figure 3a shows that the main orientations of polycrystalline Cu_{100} and Sn_{100} exhibited Cu (111) and Sn (200), respectively. The Cu-Sn alloys show peaks that are different from those shown by elemental Cu or Sn [29–32]. For the $\text{Cu}_{87}\text{Sn}_{13}$, Cu and Sn formed solid solutions, inducing an increase in lattice spacing compared with Cu (111). The $\text{Cu}_{76}\text{Sn}_{24}$ catalyst exhibited crystalline structures of both solid solutions and intermetallic compounds, which was identified as Cu_3Sn . Meanwhile, $\text{Cu}_{55}\text{Sn}_{45}$ comprised Cu_3Sn and SnO_2 [33, 34]. After CO_2 reduction at -0.89 V vs. RHE for 30 min, Cu-Sn alloy catalysts showed changes in X-ray diffraction peaks. These structural changes are attributed to the diffusion of Cu and Sn upon the application of a potential [27, 28].

The chemical bonding states of Cu 2p and Sn 3d in the alloys were analyzed by XPS before and after CO_2 reduction (Fig. 4). The chemical state of Cu on Cu_{100} and the Cu-Sn alloy catalysts was CuO (934 eV). For Sn_{100} , the Cu 2p peak is attributed to the substrate and the diffusion of Cu to Sn; this is similar to the AES result. For Sn 3d, $\text{Cu}_{87}\text{Sn}_{13}$ and $\text{Cu}_{76}\text{Sn}_{24}$ showed the same oxidation state (485.6 eV), consisting of a high percentage of SnO. On the other hand, the Sn 3d peaks of $\text{Cu}_{55}\text{Sn}_{45}$ and Sn_{100} shifted to high binding energy (486.0 eV), consisting of higher percentages of SnO_2 than in $\text{Cu}_{87}\text{Sn}_{13}$ and

Table 2 Relative composition ratios on the surfaces of the prepared catalysts, as per AES measurements

	Relative composition ratio (%)									Cu%
	Cu	Sn	C	O	Si	K	P	N	S	
Sn_{100}	2.2	30.0	4.4	42.5	–	18.5	2.4	–	–	
$\text{Sn}_{100}\text{-AR}^a$	5.8	44.4	10.7	39.1	–	–	–	–	–	
$\text{Cu}_{55}\text{Sn}_{45}$	25.2	20.8	14.1	37.4	2.5	–	–	–	–	55
$\text{Cu}_{55}\text{Sn}_{45}\text{-AR}^a$	29.2	21.8	13.0	34.0	2.0	–	–	–	–	57
$\text{Cu}_{76}\text{Sn}_{24}$	41.3	12.9	14.6	31.2	–	–	–	–	–	76
$\text{Cu}_{76}\text{Sn}_{24}\text{-AR}^a$	43.7	10.0	19.6	26.7	–	–	–	–	–	81
$\text{Cu}_{87}\text{Sn}_{13}$	50.3	7.3	15.0	27.4	–	–	–	–	–	87
$\text{Cu}_{87}\text{Sn}_{13}\text{-AR}^a$	48.0	6.1	21.4	24.5	–	–	–	–	–	89
Cu_{100}	49.8	–	22.6	21.1	–	–	–	4.9	1.6	
$\text{Cu}_{100}\text{-AR}^a$	44.9	–	25.8	18.2	–	–	–	10.1	1.1	

^a After CO_2 reduction in 0.1 M KHCO_3 at -0.89 V vs. RHE

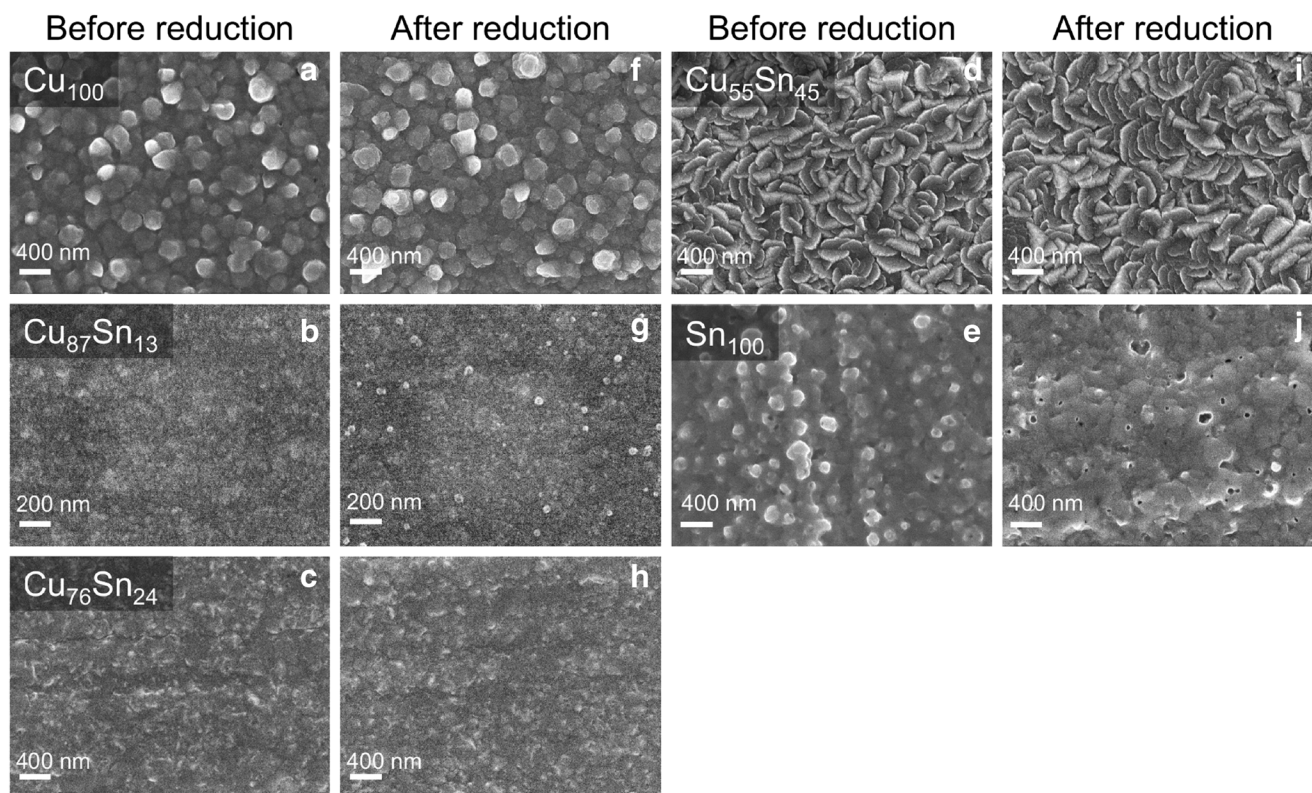


Fig. 2 SEM images of the prepared catalysts before CO₂ reduction: **a** Cu₁₀₀; **b** Cu₈₇Sn₁₃; **c** Cu₇₆Sn₂₄; **d** Cu₅₅Sn₄₅; **e** Sn₁₀₀ deposited on Cu plate. SEM images of the prepared catalysts after CO₂ reduction: **f** Cu₁₀₀; **g** Cu₈₇Sn₁₃; **h** Cu₇₆Sn₂₄; **i** Cu₅₅Sn₄₅; **j** Sn₁₀₀ deposited on Cu plate

Cu₇₆Sn₂₄ [35, 36]. Hence, the difference in the oxidation state of Sn might affect the selectivity for CO₂RR. Apart from Cu₁₀₀, the other samples showed very little difference in the Sn 3d and Cu 2p spectra before and after CO₂ reduction at – 0.89 V vs. RHE for 30 min. The Cu state in Cu₁₀₀ became Cu⁰ and CuO upon reduction from the Cu₂O state during CO₂ reduction. These results clearly suggest that the changes in morphology and crystal structure were not affected by the chemical bonding states of Cu and Sn.

CO₂ Reduction on Cu-Sn Alloy Catalysts

The CO₂ electroreduction on the prepared catalysts was conducted in a custom-made electrolysis cell (Fig. 1) for 1800 s at applied potentials ranging from – 0.69 to – 1.09 V vs. RHE. The FE values for products by CO₂ electroreduction are shown in Fig. 5. The product distribution obtained with the Cu deposition catalyst was similar to that for a reported Cu electrode and distinct from an oxide-derived Cu electrode

Fig. 3 XRD patterns of the prepared catalysts before CO₂ reduction. **a** XRD patterns of the prepared catalysts after CO₂ reduction in 0.1 M KHCO₃ at – 0.89 V vs. RHE. **b** Crystal structures of Cu₈₇Sn₁₃ were identified as solid solutions. Cu₇₆Sn₂₄ consists of Cu₃Sn as intermetallic compounds and solid solutions. For Cu₅₅Sn₄₅, Cu₃Sn and SnO₂ were identified as components

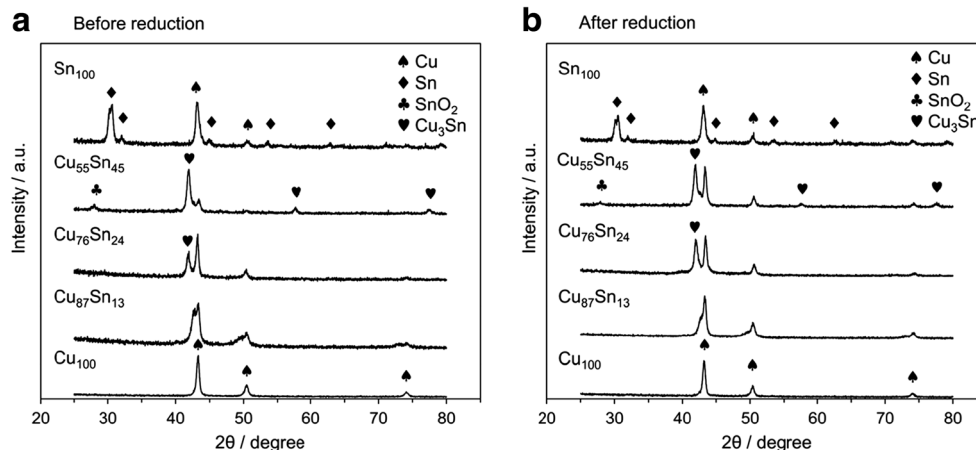
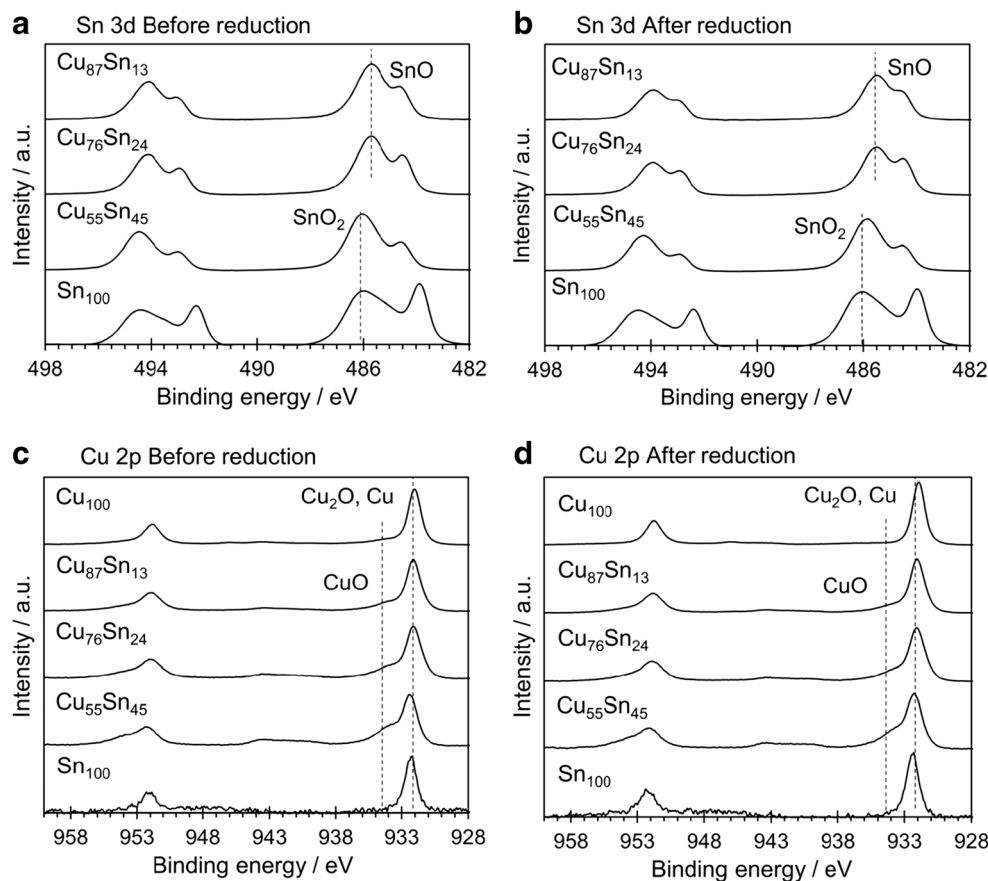


Fig. 4 XPS spectra. **a** Sn 3d spectra of $\text{Cu}_{87}\text{Sn}_{13}$, $\text{Cu}_{76}\text{Sn}_{24}$, $\text{Cu}_{55}\text{Sn}_{45}$, and Sn before reduction. **b** Sn 3d spectra after reduction. **c** Cu 2p spectra Cu_{100} , $\text{Cu}_{87}\text{Sn}_{13}$, $\text{Cu}_{76}\text{Sn}_{24}$, $\text{Cu}_{55}\text{Sn}_{45}$, and Sn before reduction. **d** Cu 2p spectra after reduction. The broken line indicates the position of each chemical bonding state: SnO_2 , SnO, CuO, Cu_2O , and Cu



(Fig. 5a) [7, 8, 16, 37]. FE for H_2 decreased with increasing applied potential; production of CH_4 and C_2H_4 was confirmed at -0.79 V vs. RHE and it showed FE of 36% at -1.09 V. FE values for CO and HCOO^- presented the same tendency, FE for HCOO^- being higher than that for CO at all applied potentials. These results showed that the Cu electrodeposition electrode leads to poor selectivity toward CO and HCOO^- . On the other hand, the Sn electrodeposition catalyst showed high FE for HCOO^- (Fig. 5e), in agreement with other research on CO_2 electroreduction with Sn electrode [24, 25]. Sn_{100} exhibited similar FE for H_2 and HCOO^- at -0.69 V; FE for H_2 decreased with increasing applied potential, while FE for HCOO^- remarkably increased to 87.5% at -1.09 V. As mentioned earlier, it is evident that the selectivity of CO production on the Sn_{100} electrode is poor.

The prepared Cu-Sn alloy catalysts exhibited different selectivities for CO_2RR . All Cu-Sn alloys can suppress HER, suggesting that the presence of Sn within the alloy by binding strongly to the surface H [23]. In $\text{Cu}_{87}\text{Sn}_{13}$, the selectivity of CO production was increased and maximum FE for CO was 59.5% at -0.99 V vs. RHE (Fig. 5b). However, the FE for CO did not change significantly with increasing applied potential. $\text{Cu}_{87}\text{Sn}_{13}$ showed a decreasing trend for H_2 generation with increasing potential. HCOO^- production shows a trend opposite to that for H_2 formation, and exhibited 12.3% FE at

-1.09 V. $\text{Cu}_{87}\text{Sn}_{13}$ produced very little hydrocarbons compared to Cu_{100} , and its maximum FE was 1.2% at -1.09 V. From the differences in selectivity, it is clear that the crystal structure significantly affected the selectivity for CO_2RR . More specifically, the formation of solid solutions affects the binding energy or binding pattern of CO_2 and its reaction intermediates. Additionally, when CO formed mainly, it may be suspected that the binding energy against surface CO ($^*\text{CO}$) gets lowered as compared to that of Cu. This decrease in binding energy is considered to depend on the lattice spacing of Cu (111) or changing surface electron density, or both.

The CO_2 reduction behavior of $\text{Cu}_{76}\text{Sn}_{24}$ was intermediate between those of $\text{Cu}_{87}\text{Sn}_{13}$ and $\text{Cu}_{55}\text{Sn}_{45}$ (Fig. 5c). From -0.69 to -0.89 V, the FE for the products showed trends similar to $\text{Cu}_{87}\text{Sn}_{13}$. At over -0.89 V, HCOO^- production increased dramatically, and it has nearly the same FE as that of CO at -1.09 V. H_2 formation decreased with increasing applied potential, same as for other electrodes. These characteristics suggest that $\text{Cu}_{76}\text{Sn}_{24}$, which consists of Cu_3Sn and solid solutions, was present at different reactive sites for CO_2 reduction on applying potential. At a low applied potential, the Cu site that originated in Cu_3Sn and solid solutions involved CO production. On the other hand, at a high applied potential, HCOO^- production occurring from the Sn site originated from Cu_3Sn . The FE for CO of $\text{Cu}_{87}\text{Sn}_{13}$ and $\text{Cu}_{76}\text{Sn}_{24}$ suggested

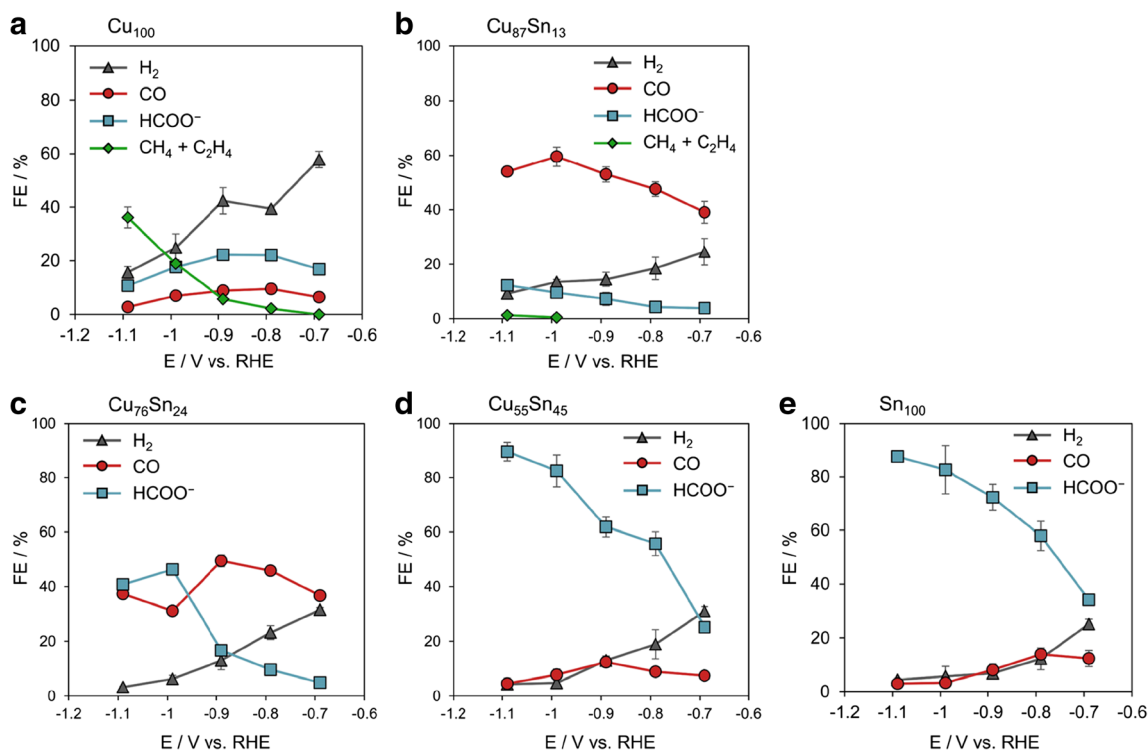


Fig. 5 Faradaic efficiency of CO₂ electroreduction products as a function of potential. **a** Cu₁₀₀; **b** Cu₈₇Sn₁₃; **c** Cu₇₆Sn₂₄; **d** Cu₅₅Sn₄₅; **e** Sn₁₀₀ deposited on Cu plate. Electrolyte, 0.1 M KHCO₃

that CO production was closely related to the Cu lattice spacing and electron density.

The product distribution using the Cu₅₅Sn₄₅ alloy electrode was close to that obtained with the Sn₁₀₀ electrode (Fig. 5d). This suggests that the Cu₃Sn structure has no effects on the selectivity for CO₂RR. Another possible factor affecting CO₂RR could be the chemical binding state of Sn within the alloys. The crystal structures of SnO₂ and Sn were observed by XRD analysis of Cu₅₅Sn₄₅ (Fig. 3). Additionally, the XPS results (Fig. 4) show that the binding energy of Sn 3d, attributed to SnO_x, was the same as that of Sn₁₀₀; however, it was different from that of Cu₈₇Sn₁₃ and Cu₇₆Sn₂₄. In fact, the FE for HCOO⁻ depends on the oxidation state of Sn [26]. From these results, it is believed that the oxidation state of Sn, rather than the crystal structure of alloy at Cu₅₅Sn₄₅, strongly affects the formation of HCOO⁻.

Figure 6 shows the total current density and partial current density of H₂, CO, and HCOO⁻ during CO₂ reduction against the applied potentials. The current density was calculated from the geometric surface area (2.75 cm²). The j_{CO} and j_{HCOO^-} values of each electrode showed the same trend as did the FE. We discuss the relationship between the selectivity, current density, and charge transfer resistance (CT resistance) in the following sections.

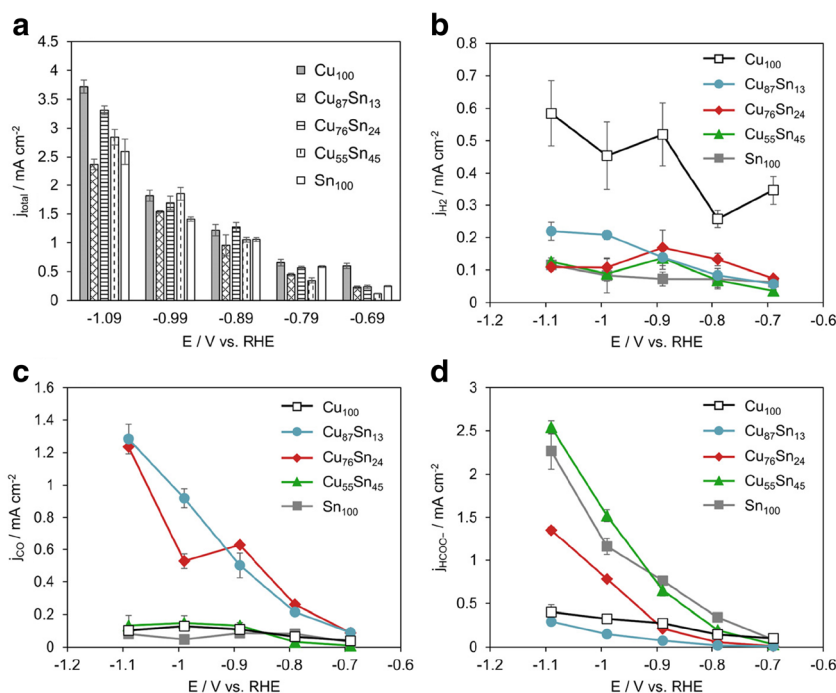
EIS Measurements on Cu-Sn Alloy

EIS measurements were performed under the same conditions as those for the CO₂RR at -0.89 and -1.09 V

vs. RHE; the obtained results were illustrated using the Cole-Cole plot. According to Fig. 7a and c, the low value in the x-axis indicates the solution resistance, and the diameter of the semicircle indicates the CT resistance (Fig. 7b, d). The CT resistance was found to be closely related to the current density; the catalysts with low CT resistance showed an increase in j_{total} , except for Cu₁₀₀.

Cu₁₀₀ exhibited high current density despite the large CT resistance, because it showed a high FE for multi-electron reduction products, including CH₄ and C₂H₄ (Fig. 5a). The CT resistance of Cu₅₅Sn₄₅ and Sn₁₀₀, which had a high j_{HCOO^-} , was lower than that of the other catalysts at -0.89 and -1.09 V. This suggested that the resistance of the reaction pathway for the generation of HCOO⁻ from CO₂ was low; that is, CO₂RR is not routed through the adsorption of CO₂ and its intermediates on Cu₅₅Sn₄₅ and Sn₁₀₀. At -1.09 V, the CT resistance of Cu₅₅Sn₄₅ was lower than that of Sn₁₀₀ and this result corresponded to the highest j_{HCOO^-} . Cu₇₆Sn₂₄ exhibited the same CT resistance as Sn₁₀₀ at -0.89 and -1.09 V, but the j_{total} , j_{CO} , and j_{HCOO^-} values were different from those of Sn₁₀₀. This result suggests that the Sn sites originating from Cu₃Sn possessed high selectivity for HCOO⁻ and decreased CT resistance. The CT resistance of Cu₈₇Sn₁₃ at both applied potentials was larger than that of the other Cu-Sn alloy, but the j_{total} value was smaller. Based on these results, we speculated that CO₂RR on

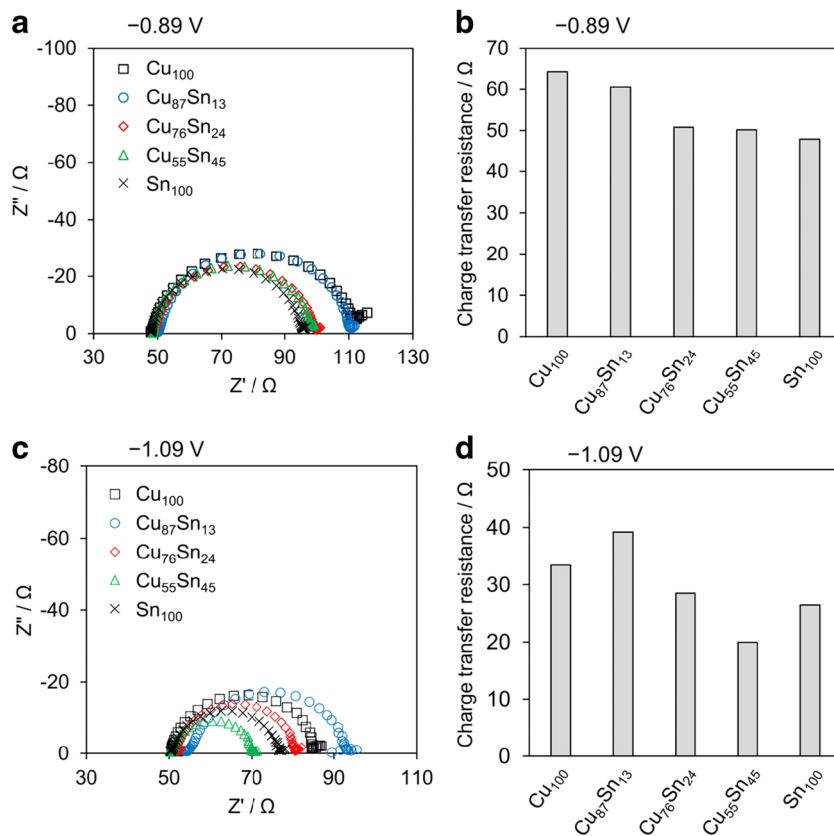
Fig. 6 Total current density for CO_2 electroreduction as a function of potential on Cu_{100} , $\text{Cu}_{87}\text{Sn}_{13}$, $\text{Cu}_{76}\text{Sn}_{24}$, $\text{Cu}_{55}\text{Sn}_{45}$, and Sn_{100} . **a** Partial current density of the products from CO_2 reduction on each catalyst; **b** H_2 ; **c** CO ; **d** HCOO^-



solid solutions progresses through the CO_2 reaction intermediates binding to the catalyst surface. $\text{Cu}_{87}\text{Sn}_{13}$ exhibited a larger CT resistance as compared to $\text{Cu}_{76}\text{Sn}_{24}$ at

both potentials, probably because of the increase in the amount of adsorbed intermediates as compared to $\text{Cu}_{87}\text{Sn}_{13}$.

Fig. 7 Cole-Cole plot for Cu_{100} , $\text{Cu}_{87}\text{Sn}_{13}$, $\text{Cu}_{76}\text{Sn}_{24}$, $\text{Cu}_{55}\text{Sn}_{45}$, and Sn_{100} during electrochemical CO_2 reduction in 0.1 M KHCO_3 at **a** -0.89 and **c** -1.09 V vs. RHE. Charge transfer resistance of each electrode at **b** -0.89 and **d** -1.09 V vs. RHE



CO₂RR Mechanism for Each Cu-Sn Alloy

CO₂RR mechanism on Cu surface has been elucidated employing DFT calculations [18, 38–40]. Briefly, CO₂ first adsorbs and reduces on Cu surface by accepting an electron and proton, and then forms surface HOCO (*HOCO), which is adsorbed on the electrode. HCOO[−] is generated to desorb *HOCO at this stage, and with the progression of the reduction reaction, adsorbed *CO and H₂O are generated. Similarly, CO is generated by the desorption of *CO, and adsorbed surface HCO (*HCO) is generated by the progress of the reduction reaction. Furthermore, with the progression of the reduction reaction, the *HCO intermediate becomes reduced and generates CH₄ and CH₃OH. Generation of C₂ compounds require dimer formation from intermediates like *CO [18]. The prepared Cu₁₀₀ electrode is considered to perform according to the above mechanism.

CO₂RR on Cu₈₇Sn₁₃ is suggested to behave the same as the adsorbed phase of Cu₁₀₀ by EIS (Fig. 7). However, Cu₁₀₀ and Cu₈₇Sn₁₃ have different selectivities for CO₂ reduction and the main product on Cu₈₇Sn₁₃ was CO, because Cu₈₇Sn₁₃ was a solid solution which consists of Cu and Sn. It seems that formation of solid solutions increases the lattice spacing of Cu (111) and changes surface electron density. This surface characteristic change might lower the binding energy of the reaction intermediate *CO. Furthermore, Cu₈₇Sn₁₃ inhibits further *CO reduction at −1.09 V, thereby enhancing CO formation [7].

Meanwhile, the proposed reaction pathway for HCOO[−] formation on Sn involved a reaction with CO₂ to generate surface H (*H) [38, 41]. In this study, the Sn₁₀₀ electrode might react according to the abovementioned pathway, because Sn₁₀₀ exhibits a lower CT resistance than Cu₁₀₀ (Fig. 7). Among the prepared alloy catalysts, Cu₅₅Sn₄₅ follows the same mechanism because its CO₂RR selectivity and EIS results are similar to those of Sn₁₀₀. These results suggest that the active site of CO₂RR is Sn, i.e., the surface oxidation state of Sn, rather than the crystal structure of Cu₅₅Sn₄₅, is the major factor contributing to CO₂RR.

In contrast, Cu₇₆Sn₂₄ exhibited a CT resistance similar to that of Sn₁₀₀ and Cu₅₅Sn₄₅, but the selectivity for CO₂RR was different from theirs. Discussion on Cu₇₆Sn₂₄ is difficult because the Cu and Sn sites in Cu₃Sn affect CO₂RR selectivity (Fig. 5c). The EIS results suggested that surface Sn affects the adsorbed state and the reaction pathway.

Conclusion

We prepared Cu-Sn alloy catalytic electrodes through the simple electrodeposition method for electrochemical CO₂ reduction. The Cu-Sn alloy catalysts can control the selectivity for CO and HCOO[−] formation from CO₂ by changing the crystal

structure. In addition, these catalysts strongly inhibit HER compared to Cu due to the presence of Sn. Cu₈₇Sn₁₃ showed high selectivity toward CO formation, such that its faradaic efficiency was 60% at −0.99 V vs. RHE differing from electrodeposited Cu catalysts. The surface analyses revealed that solid solutions play an important role in CO formation upon CO₂ reduction, because solid solution formation weakens the binding energy between the Cu-Sn alloy and the reaction intermediate *CO. On the other hand, Cu₅₅Sn₄₅ showed 89.5% of FE for HCOO[−] at −1.09 V; this result was nearly the same as that for Sn₁₀₀ (87.5%). These results indicate that increasing surface SnO₂ promotes HCOO[−] rather than the presence of intermetallic compounds. The Cu₇₆Sn₂₄ alloy exhibited properties intermediate between Cu₈₇Sn₁₃ and Cu₅₅Sn₄₅ at −1.09 V, i.e., 37.4% FE for CO and 40.8% FE for HCOO[−]. This result suggested that there may be two active sites: Cu and Sn in Cu₃Sn, due to which the selectivity behavior of CO₂RR differs depending on applied potential.

Acknowledgements This research has been partly supported by the Advanced Catalytic Transformation Program for Carbon Utilization (ACT-C), Japan Science and Technology Agency (JST), and Research Center for Advanced Eco-Fitting Technology, Kyushu Institute of Technology.

Open Access This article is distributed under the terms of the Creative Commons Attribution 4.0 International License (<http://creativecommons.org/licenses/by/4.0/>), which permits unrestricted use, distribution, and reproduction in any medium, provided you give appropriate credit to the original author(s) and the source, provide a link to the Creative Commons license, and indicate if changes were made.

References

1. S.J. Davis, K. Caldeira, H.D. Matthews, Future CO₂ emissions and climate change from existing energy infrastructure. *Science* (80-) **329**, 1330–1333 (2010)
2. M. Mikkelsen, M. Jørgensen, F.C. Krebs, The teraton challenge. A review of fixation and transformation of carbon dioxide. *Energy Environ. Sci.* **3**, 43–81 (2010)
3. A. Sanna, M. Uibu, G. Caramanna, R. Kuusik, M.M. Maroto-Valer, A review of mineral carbonation technologies to sequester CO₂. *Chem. Soc. Rev.* **43**, 8049–8080 (2014)
4. Y.A. Daza, R.A. Kent, M.M. Yung, J.N. Kuhn, Carbon dioxide conversion by reverse water-gas shift chemical looping on perovskite-type oxides. *Ind. Eng. Chem. Res.* **53**, 5828–5837 (2014)
5. H. Noda, S. Ikeda, Y. Oda, K. Imai, M. Maeda, K. Ito, S. Ideka, Y. Oda, K. Imai, M. Maeda, I. Kaname, Electrochemical reduction of carbon dioxide at various metal electrodes in aqueous potassium hydrogen carbonate solution. *Bull. Chem. Soc. Jpn.* **63**, 2459–2462 (1990)
6. Y. Hori, H. Wakebe, T. Tsukamoto, O. Koga, Electrocatalytic process of CO selectivity in electrochemical reduction of CO₂ at metal electrodes in aqueous media. *Electrochim. Acta* **39**, 1833–1839 (1994)
7. K.P. Kuhl, T. Hatsukade, E.R. Cave, D.N. Abram, J. Kibsgaard, T.F. Jaramillo, Electrocatalytic conversion of carbon dioxide to

- methane and methanol on transition metal surfaces. *J. Am. Chem. Soc.* **136**, 14107–14113 (2014)
8. K.P. Kuhl, E.R. Cave, D.N. Abram, T.F. Jaramillo, New insights into the electrochemical reduction of carbon dioxide on metallic copper surfaces. *Energy Environ. Sci.* **5**, 7050–7059 (2012)
 9. M. Gattrell, N. Gupta, A. Co, A review of the aqueous electrochemical reduction of CO₂ to hydrocarbons at copper. *J. Electroanal. Chem.* **594**, 1–19 (2006)
 10. A. Peterson, J. Nørskov, Activity descriptors for CO₂ electroreduction to methane on transition metal catalysts. *J. Phys. Chem. Lett.* **3**, 251–258 (2012)
 11. S.A. Akhade, W. Luo, X. Nie, A. Asthagiri, M.J. Janik, Theoretical insight on reactivity trends in CO₂ electroreduction across transition metals. *Catal. Sci. Technol.* **6**, 1042–1053 (2015)
 12. H.K. Lim, H. Shin, W.A. Goddard, Y.J. Hwang, B.K. Min, H. Kim, Embedding covalency into metal catalysts for efficient electrochemical conversion of CO₂. *J. Am. Chem. Soc.* **136**, 11355–11361 (2014)
 13. Y. Hori, I. Takahashi, O. Koga, N. Hoshi, Electrochemical reduction of carbon dioxide at various series of copper single crystal electrodes. *J. Mol. Catal. A Chem.* **199**, 39–47 (2003)
 14. N. Hoshi, M. Kato, Y. Hori, Electrochemical reduction of CO₂ on single crystal electrodes of silver. *J. Electroanal. Chem.* **440**, 283–286 (1997)
 15. D. Kim, S. Lee, J.D. Ocon, B. Jeong, J.K. Lee, K. Lee, J.K. Lee, Insights into autonomously formed oxygen-evacuated Cu₂O electrode for the selective production of C₂H₄ from CO₂. *Phys. Chem. Chem. Phys.* **17**, 1–9 (2014)
 16. R. Kas, R. Kortlever, A. Milbrat, M.T.M. Koper, G. Mul, J. Baltrusaitis, Electrochemical CO₂ reduction on Cu₂O-derived copper nanoparticles: controlling the catalytic selectivity of hydrocarbons. *Phys. Chem. Chem. Phys.* **16**, 12194–12201 (2014)
 17. P. Hirunsit, Electroreduction of carbon dioxide to methane on copper, copper-silver, and copper-gold catalysts: a DFT study. *J. Phys. Chem. C* **117**, 8262–8268 (2013)
 18. P. Hirunsit, W. Soodsawang, J. Limtrakul, CO₂ electrochemical reduction to methane and methanol on copper-based alloys: theoretical insight. *J. Phys. Chem. C* **119**, 8238–8249 (2015)
 19. T. Adit Maark, B.R.K. Nanda, CO and CO₂ electrochemical reduction to methane on Cu, Ni, and Cu₃Ni (211) surfaces. *J. Phys. Chem. C* **120**, 8781–8789 (2016)
 20. R. Kortlever, I. Peters, S. Koper, M.T.M. Koper, Electrochemical CO₂ reduction to formic acid at low overpotential and with high faradaic efficiency on carbon-supported bimetallic Pd-Pt nanoparticles. *ACS Catal.* **5**, 3916–3923 (2015)
 21. D. Ren, B.S.-H. Ang, B.S. Yeo, Tuning the selectivity of carbon dioxide electroreduction toward ethanol on oxide-derived Cu_xZn catalysts. *ACS Catal.* 8239–8247 (2016)
 22. A. Jedidi, S. Rasul, D. Masih, L. Cavallo, K. Takanabe, Generation of Cu–In alloy surfaces from CuInO₂ as selective catalytic sites for CO₂ electroreduction. *J. Mater. Chem. A* **3**, 19085–19092 (2015)
 23. S. Sarfraz, A.T. Garcia-Esparza, A. Jedidi, L. Cavallo, K. Takanabe, Cu–Sn bimetallic catalyst for selective aqueous electroreduction of CO₂ to CO. *ACS Catal.* **6**, 2842–2851 (2016)
 24. W. Lv, R. Zhang, P. Gao, L. Lei, Studies on the faradaic efficiency for electrochemical reduction of carbon dioxide to formate on tin electrode. *J. Power Sources* **253**, 276–281 (2014)
 25. C. Zhao, J. Wang, Electrochemical reduction of CO₂ to formate in aqueous solution using electro-deposited Sn catalysts. *Chem. Eng. J.* **293**, 161–170 (2016)
 26. Y. Chen, M.W. Kanan, Tin oxide dependence of the CO₂ reduction efficiency on tin electrodes and enhanced activity for tin/tin oxide thin-film catalysts. *J. Am. Chem. Soc.* **134**, 1986–1989 (2012)
 27. M. Onishi, H. Fujibuchi, Reaction-diffusion in the Cu–Sn system. *J. Chem. Inf. Model.* **16**, 539–547 (1975)
 28. Y. Yuan, Y. Guan, D. Li, N. Moelans, Investigation of diffusion behavior in Cu–Sn solid state diffusion couples. *J. Alloys Compd.* **661**, 282–293 (2016)
 29. T. Yamamoto, T. Nohira, R. Hagiwara, A. Fukunaga, S. Sakai, K. Nitta, S. Inazawa, Improved cyclability of Sn–Cu film electrode for sodium secondary battery using inorganic ionic liquid electrolyte. *Electrochim. Acta* **135**, 60–67 (2014)
 30. A. Survila, Z. Mockus, S. Kanapeckaitė, D. Bražinskienė, R. Juškėnas, Surfactant effects in Cu–Sn alloy deposition. *J. Electrochem. Soc.* **159**, D296–D302 (2012)
 31. A. Survila, Z. Mockus, S. Kanapeckaitė, V. Jasulaitienė, R. Juškėnas, Codeposition of copper and tin from acid sulphate solutions containing gluconic acid. *J. Electroanal. Chem.* **647**, 123–127 (2010)
 32. B.H. Bui, S. Kim, Preparation of Cu–Sn alloy foam by electrodeposition in acid solution. *J. Electrochem. Soc.* **162**, D15–D19 (2014)
 33. W.X. Lei, Y. Pan, Y.C. Zhou, W. Zhou, M.L. Peng, Z.S. Ma, CNTs–Cu composite layer enhanced Sn–Cu alloy as high performance anode materials for lithium-ion batteries. *RSC Adv.* **4**, 3233 (2014)
 34. T. Shukla, Synthesis of tin oxide thick film and its investigation as a LPG sensor at room temperature. *J. Sens. Technol.* **2**, 102–108 (2012)
 35. Y. Kang, J. Park, Y.-C. Kang, Surface characterization of CuSn thin films deposited by RF co-sputtering method. *Surf. Interface Anal.* **48**, 963–968 (2016)
 36. S. Naille, R. Dedryvère, H. Martinez, S. Leroy, P.-E. Lippens, J.-C. Jumas, D. Gonbeau, XPS study of electrode/electrolyte interfaces of η-Cu₆Sn₅ electrodes in Li-ion batteries. *J. Power Sources* **174**, 1086–1090 (2007)
 37. A.D. Handoko, C.W. Ong, Y. Huang, Z.G. Lee, L. Lin, G.B. Panetti, B.S. Yeo, Mechanistic insights into the selective electroreduction of carbon dioxide to ethylene on Cu₂O-derived copper catalysts. *J. Phys. Chem. C* **120**, 20058–20067 (2016)
 38. T. Cheng, H. Xiao, W.A. Goddard, Reaction mechanisms for the electrochemical reduction of CO₂ to CO and formate on the Cu(100) surface at 298 K from quantum mechanics free energy calculations with explicit water. *J. Am. Chem. Soc.* **138**, 13802–13805 (2016)
 39. W. Luo, X. Nie, M.J. Janik, A. Asthagiri, Facet dependence of CO₂ reduction paths on Cu electrodes. *ACS Catal.* **6**, 219–229 (2016)
 40. X. Nie, W. Luo, M.J. Janik, A. Asthagiri, Reaction mechanisms of CO₂ electrochemical reduction on Cu(111) determined with density functional theory. *J. Catal.* **312**, 108–122 (2014)
 41. C. Cui, H. Wang, X. Zhu, J. Han, Q. Ge, A DFT study of CO₂ electrochemical reduction on Pb(211) and Sn(112). *Sci. China Chem.* **58**, 607–613 (2015)